




Research Article

Methylene Blue Adsorption BY UV-Treated Graphene Oxide Nanoparticles (UV/n-GO): Modeling and Optimization Using Response Surface Methodology and Artificial Neural Networks

M. Venkata Ratnam ¹, Manikkampatti Palanisamy Murugesan ²,
Srikanth Komarabathina,³ S. Samraj,⁴ Mohammedsani Abdulkadir ¹,
and Muktar Abdu Kalifa¹

¹Department of Chemical Engineering, Mettu University, Metu, Ethiopia

²Department of Food Technology, Excel Engineering College, Komarapalayam, TamilNadu, India

³Department of Chemical Engineering, KIoT, Wollo University, Kombolcha, Ethiopia

⁴Department of Chemical Engineering, MVJ College of Engineering, Bangalore, India

Correspondence should be addressed to M. Venkata Ratnam; mvratnam81@gmail.com

Received 1 March 2022; Revised 22 July 2022; Accepted 13 September 2022; Published 29 September 2022

Academic Editor: Sébastien Déon

Copyright © 2022 M. Venkata Ratnam et al. This is an open access article distributed under the Creative Commons Attribution License, which permits unrestricted use, distribution, and reproduction in any medium, provided the original work is properly cited.

To mitigate the negative effects of pollution produced by the growing levels of pollutants in the environment, research and development of novel and more effective materials for the treatment of pollutants originating from a variety of industrial sources should be prioritized. In this research, a UV-irradiated nano-graphene oxide (UV/n-GO) was developed and studied for methylene blue (MB) adsorption. Furthermore, the batch adsorption studies were modelled using response surface modelling (RSM) and artificial neural networks (ANNs). Investigations employing FTIR, XRD, and SEM were carried out to characterize the adsorbent. The best MB removal of 95.81% was obtained at a pH of 6, a dose of 0.4 g/L, an MB concentration of 25 mg/L, and a period of 40 min. This was accomplished with a desirability score of 0.853. A three-layer backpropagation network with an ideal structure of 4-4-1 was used to create an ANN model. The R^2 and MSE values determined by comparing the modelled data with the experimental data were 0.9572 and 0.00012, respectively. The % MB removal predicted by ANN was 94.76%. The kinetics of adsorption corresponded well with the pseudo-second-order model ($R^2 > 0.97$). According to correlation coefficients, the order of adsorption isotherm models is Redlich–Peterson > Temkin > Langmuir > Freundlich. Thermodynamic investigations show that MB adsorption was both spontaneous and endothermic.

1. Introduction

Water resources are becoming polluted as industrialization expands. The public is endangered by the majority of enterprises that dump wastewater into surrounding water sources [1]. The biggest contributors to wastewater generation are textile, leather, and tanning industries, breweries, oil mills, food processing, and chemical industries. The textile industry creates a significant amount of liquid waste [2]. In textile manufacture, up to 2000 different chemicals, ranging from dyes to transfer agents, are used. A typical

textile mill (making around 8000 kg of cloth per day) utilizes approximately 1.6 million gallons of water every day. In addition, this may generate up to 200–350 m³ of effluent per ton of finished products. These textile effluents contain both organic and inorganic pollutants [3, 4]. Not all colors that are applied to clothing are fixed to them during the dyeing process, and a large portion of these colors always remain unfixed to the fabric and are washed off. Significant levels of unfixed dyes have been found in textile effluents. Severe effects on local water systems have already been observed in certain areas. This emphasizes the significance of proper

water treatment processes for long-term water consumption [2, 5, 6]. Such effluents include high levels of dyes and chemicals, some of which are nonbiodegradable and carcinogenic, posing significant environmental concerns. These effluents were treated using a variety of primary, secondary, and tertiary treatment methods [5]. However, these methods have not been shown to be successful in removing dyes completely [7, 8]. Because of the need for replenishing water for new purposes, wastewater purification is practically essential for achieving the desired level of purity.

Adsorption is the simplest and most efficient technique due to its low cost, excellent separation capability, the availability of a variety of low-cost adsorbents, and the absence of secondary pollutant formation [9–12]. Adsorption may also be employed to remove organic, inorganic, and biological pollutants, both soluble and insoluble [13–15]. The adsorbents' porous nature and wide surface area are regarded as the key characteristics responsible for dye removal. Hence, adsorption proved to be a very effective and lucrative method for eliminating pollutants from industrial effluents. In dealing with organic pollutants in water, such as dyes, the development of ecologically friendly adsorbents is becoming increasingly crucial.

Nanotechnology has the potential to solve problems in nearly every field of science and technology [16]. Materials' characteristics at the nanoscale differ greatly from those of bulk materials. Because of the importance of water quality and the rising benefits of nanotechnology, encouraging the use of nanomaterials opens the door to the development of efficient solutions to worldwide water pollution. The adsorbent's surface functional groups and pore structure have a significant impact on its adsorption process applicability. Nanomaterials have been shown to be efficient wastewater treatment materials due to qualities such as high surface activity and reusability. Metal oxide nanoparticles have recently received a lot of attention as better environmental and energy materials [17].

Graphene, a remarkable two-dimensional carbon-based substance with atomic thicknesses and a high surface-to-volume ratio, has sparked widespread interest throughout the world. Graphene oxide (GO), an oxidized derivative of graphene, comprises functional groups such as hydroxyl and carboxyl groups [4, 18, 19]. Because of the presence of these functional groups, GO has a greater surface charge and is easier to disperse in solution, making it an excellent adsorbent. However, separation issues and the fact that it is hydrophobic limit its practical utilization in water. Furthermore, due to high van der Waals forces, graphene tends to cluster, resulting in a decrease in the surface area and hence a loss in adsorption efficiency [7–9, 20]. The functionalization of graphene materials appears to be an obvious answer to this challenge. As a result, researchers focused on several GO modifications, with amine functionalization emerging as the most promising. However, the price is excessively high. A basic physical treatment of UV irradiation of GO is inexpensive and effective [21]. Irradiation of graphene oxide foam promotes CO₂ adsorption [21], with a 30-fold improvement in selectivity at 100 mbar and a 7-fold increase in CO₂ capacity after 5 hrs of the UV treatment. The

UV treatment of graphene-based adsorbents can increase the efficiency of carbon capture, which might be used as a simple and low-cost pretreatment strategy. Graphene oxide surface changes will improve the adsorption efficacy. However, the literature consists primarily of surface functionalization of GO by chemical techniques, which are both costly and harmful. As a result, the current research focuses on the creation of a modified graphene adsorbent for the treatment of organic contaminants using a simple physical technique. Methylene blue (MB) is a cationic dye with a heteropolycyclic structure that prevents biological degradation and is extremely difficult to degrade into tiny inorganic molecules using conventional techniques. In humans, MB produces cyanosis, jaundice, quadriplegia, and tissue necrosis, as well as a fast heart rate, vomiting, shock, and tissue necrosis. As a result, in adsorption testing, MB is utilized as a model pollutant. The goal of this research is to develop a simple adsorbent (UV/n-GO) for MB adsorption. Scanning electron microscopy (SEM), Fourier transform infrared spectrum (FTIR), and X-ray diffraction (XRD) were used to characterize the adsorbent. Response surface methodology (RSM) and artificial neural networks (ANNs) were used to optimize the adsorption parameters. The adsorption behavior of MB on UV/n-GO, including adsorption kinetics, isotherms, and thermodynamics, was also investigated.

2. Experimental Work

2.1. Chemicals and Reagents. All chemicals of analytical grade were used for this study. Graphite flakes and methylene blue (MB) (Sigma-Aldrich), H₂SO₄, KMnO₄, and H₃PO₄ (Fisher Scientific), and H₂O₂, HCl, and NaOH (LobaChemie) were employed in this study. The experiments were performed in triplicate, and deionized water was used in the experiments.

2.2. Synthesis and Characterization of Adsorbents. Graphite was oxidized by physically agitating graphite flakes (weighing 5 g) in concentrated sulfuric acid for 30 min. After that, concentrated phosphoric acid (33 ml) was added to the mixture with mechanical stirring. After 60 min, 27 g of potassium permanganate was added as a strong oxidizing agent. To achieve total graphite oxidation, this mixture was physically churned. This was confirmed by the production of a dark brown color instead of the initial dark purplish green tint, indicating that graphite oxidation was effective. To stop the oxidation reaction, 150 ml of a 30% hydrogen peroxide solution was added to the mixture. A brilliant yellow color was visible at this point. Following this, the product was centrifuged for fifteen minutes to separate out the acid fraction, which appeared as the supernatant layer. After getting an oxidized sample, it was washed up to ten times with 1 N hydrochloric acid solution, followed by washing it with the deionized water until it reached a pH of 5. The material was then allowed to dry for two days. To undergo the UV treatment, the as-prepared n-GO was put within a UV cabinet equipped with UV lights. n-GO was exposed to

UV irradiation for periods ranging from 0.5 to 10 hrs. The light source should be switched on once the n-GO samples have been put in the UV chamber. Samples should be obtained from the UV chamber at the following intervals: 30 min, 1 hr, 2 hrs, 3 hrs, 4 hrs, 5 hrs, and 10 hrs. A UV-Vis spectrophotometer was utilized to conduct the material analysis.

2.3. Adsorption Procedure. We prepare 50 ml of dye solution in conical flasks and adjust the agitation duration (t , min.), pH of the aqueous solution, UV/n-GO dosage (w , g/L), and starting concentration of dye in the aqueous solution (C_0 , mg/L) for each sample. The samples are agitated with an ultrasonic bath that is provided. After shaking for the prescribed time, we filter the samples and dry the UV/n-GO adsorbent. Using a UV spectrophotometer, the concentration of filtered MB dye solution (liquid samples) after adsorption is determined. The % dye removal by adsorption is calculated as follows:

$$\% \text{removal} = \frac{(C_0 - C_e)}{C_0} \times 100, \quad (1)$$

where C_0 is the starting MB solution concentration and C_e denotes the MB solution's ultimate concentration after adsorption.

2.4. Modeling and Optimization. Data analysis will be performed by using Design of Experiments (DOE) software to optimize and to find the effect of combined variables on the process, and MATLAB software will be used to find the optimum conditions.

2.4.1. Experimental Design and Statistical Analysis Using CCD. RSM is a collection of mathematical and statistical approaches that are based on fitting a polynomial equation to experimental data obtained within the operable area of process variables. It is useful when many independent process factors impact a response (dependent variable) or a group of responses of interest [6]. The goal is to optimize the levels of various process variables at the same time to get the optimum system performance. The optimization process consists of four key steps: conducting statistically planned experiments, estimating the coefficients in a mathematical model, forecasting the response, and determining the model's appropriateness. Box and Wilson introduced the central composite design (CCD). The full CCD consists primarily of (1) a complete $2n$ factorial design, where n is the number of test variables, (2) n_0 centre points ($n_0 \geq 1$), and (3) two axial points on the axis of each design variable at a distance of $2n/4$ from the design centre. As a result, the total number of design points is $N = 2n + 2n + n_0$, and the five variable levels are $(-2n/4, -1, 0, +1, \text{ and } +2n/4)$. The batch adsorption study comprised finding out the effects of various parameters such as agitation time (t , min.), pH of the aqueous solution, adsorbent dosage (w , g/L), and initial concentration of dye in the

aqueous solution (C_0 , mg/L) on the Design of Experiments (DOE).

2.4.2. ANN Modelling with MATLAB. By examining the existing data, the ANN model may learn the pattern of the underlying process and then generalize what it has learnt (or the complex mathematical relationship between input and output data). An ANN model can predict any complicated system by evaluating its design. Because of the intricacy of the adsorption process, a computational intelligence-based ANN model offers greater flexibility than a statistical model, which may represent intricate datasets with nonlinearities. This is because ANN models are based on artificial neural networks. The artificial neural network (ANN) model is made up of three layers: input, hidden, and output. These layers, for example, can be utilized to anticipate the relationship between the input and output layers [22–24]. After that, the content was separated into three categories at random: learning (70%), testing (20%), and validation (10%). The learning dataset is used to train the ANN model. The testing dataset is used to evaluate the prediction capacity of the ANN model. The coefficient of determination is used as a performance metric to determine how well the ANN model operates (R^2). A variety of parameters can affect the effectiveness of the ANN model, including the number of neurons in both the hidden and output layers, as well as the shape of the transfer function. ANN computations were performed using MATLAB Toolbox, version R2021a, throughout this investigation.

3. Results and Discussion

3.1. Characterization Studies. UV light was used to reduce n-GO at varied time intervals. The analytical findings for all seven samples (samples 1–7, for time periods $t = 0.5, 1, 2, 3, 4, 5,$ and 10 hrs) are shown in Figure 1(a). The development of n-GO was demonstrated by the UV-Vis spectra of the produced sample, which is shown in Figure 1(a) and verifies the formation of nanoparticles [4, 25, 26]. UV light works as a reducing agent, and the rate of oxidation rises with time [26]. Because the material was substantially oxidized at time $t = 10$ hrs (Sample 7), time $t = 5$ hrs (Sample 6) is regarded optimal. UV/n-GO peaks were found at wavelengths ranging from 240 to 243 nm, suggesting a little shift from the n-GO sample, where the peak was seen at 230 nm. The XRD patterns of UV-treated nano-graphene oxide are shown in Figure 1(b). The experiments were performed on Rigaku Miniflex at a scan speed of $1^\circ/\text{min}$ from 10° to 80° . Scherer's equation [18] was used to calculate the crystallite size of the samples. In all situations, sharp crystalline peaks may be detected. In this study, the crystallite size was determined using the highest diffraction peaks, yielding an average crystallite size of 13.2 nm for n-GO and 12.24 nm for UV/n-GO. The UV/n-GO SEM images are shown in Figure 1(c). Surface morphology was determined using a field-emission scanning electron microscope (FESEM, Carl Zeiss NTS GmbH, Germany). UV light causes spherical aggregation of

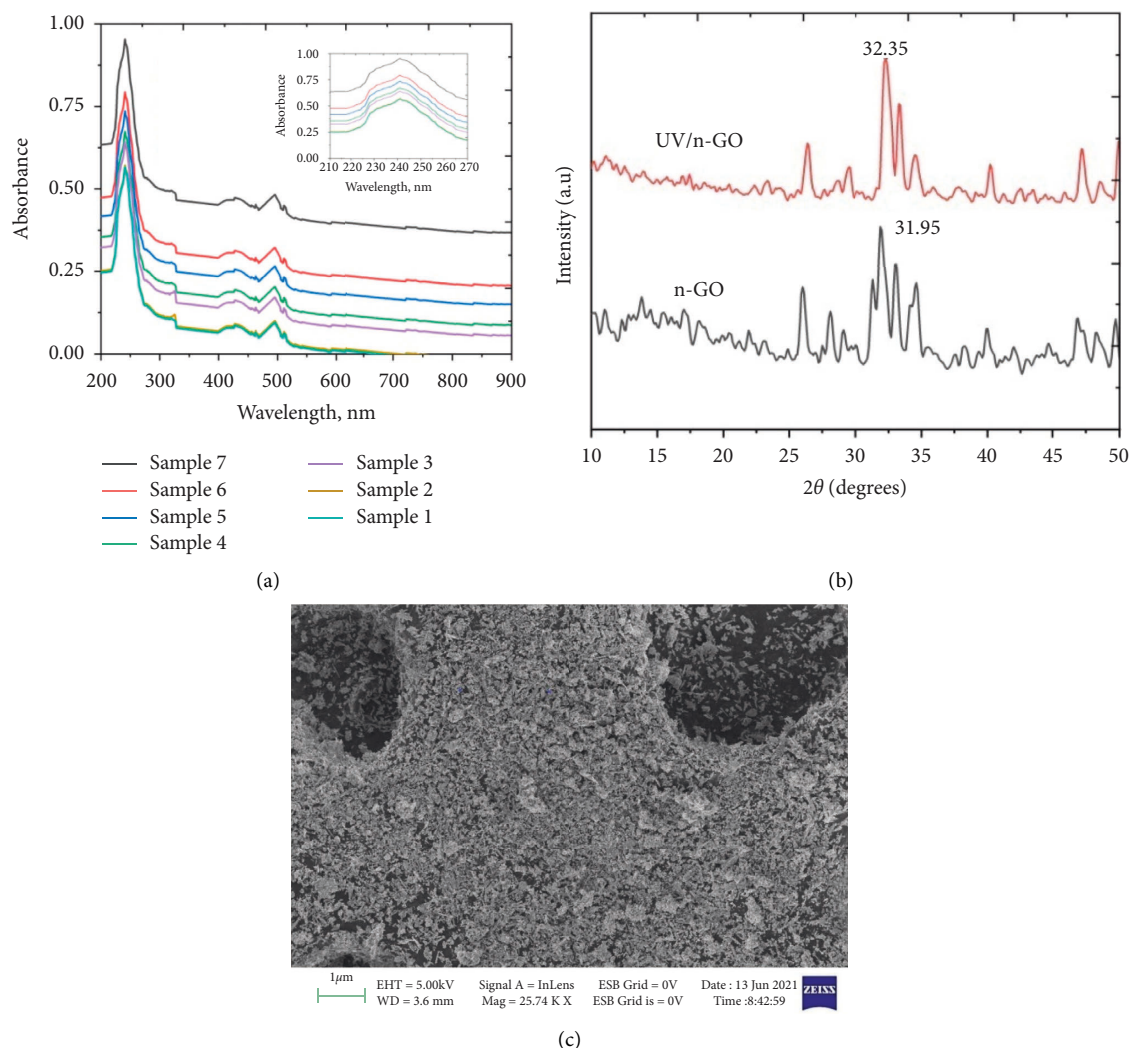


FIGURE 1: (a) UV analysis of UV/n-GO; (b) XRD of n-GO and UV/n-GO; (c) SEM image of UV/n-GO.

graphene oxide particles on rough surfaces, as seen in the images.

The use of FTIR spectroscopy to evaluate the presence of various functional groups in graphene oxide, particularly oxygen-containing functional groups, is a powerful method. Figures 2(a) and 2(b) depict the FTIR spectrum characteristics of n-GO and UV/n-GO, respectively. Stretching vibrations of OH functional groups were found at 3696 cm^{-1} in the case of n-GO. Carbonyl group (C=O) stretching vibrations were discovered at 1636 cm^{-1} , whereas alkoxy C-O stretching vibrations were discovered at 1056 cm^{-1} . At 1387 cm^{-1} , C-OH stretching bands were obtained. This matches with the existing literature findings [12, 26, 27]. FTIR spectroscopy was used to investigate the UV reduction of GO. The intensities of the peaks corresponding to -OH of UV/n-GO were lower than the intensities of graphene oxide peaks. This proved that UV light can successfully degrade graphene oxide.

3.2. Analysis of the Adsorption Parameters Using Design Expert Software. A four-factor CCD (central composite

design) and a second-order RSM were used to observe the effect of variables on dye recovery based on 30 experimental runs at various numerical values of time (A), adsorbent dose (B), initial concentration of dye solution (C), and pH (D) while keeping temperature constant at room temperature. STATISTICA Version 11.0 was used to analyze the answer (Stat-Ease, Inc). Based on Fisher's F -test, the analysis of variance (ANOVA) was utilized to perform diagnostic testing checks for the appropriateness of the suggested model. The regression coefficient (R^2) indicates the amount of variation around the mean explained by the model. The ranges of each variable studied are summarized in Table 1. The coded and uncoded levels of independent factors according to the 30 experiments corresponding to CCD along with their responses are shown in Table 2. The minimum and maximum values of the independent factors were chosen based on the literature.

3.2.1. Analysis of Variance (ANOVA). To determine whether or not the quadratic model is significantly affected by the parameters listed in the design, it was crucial to

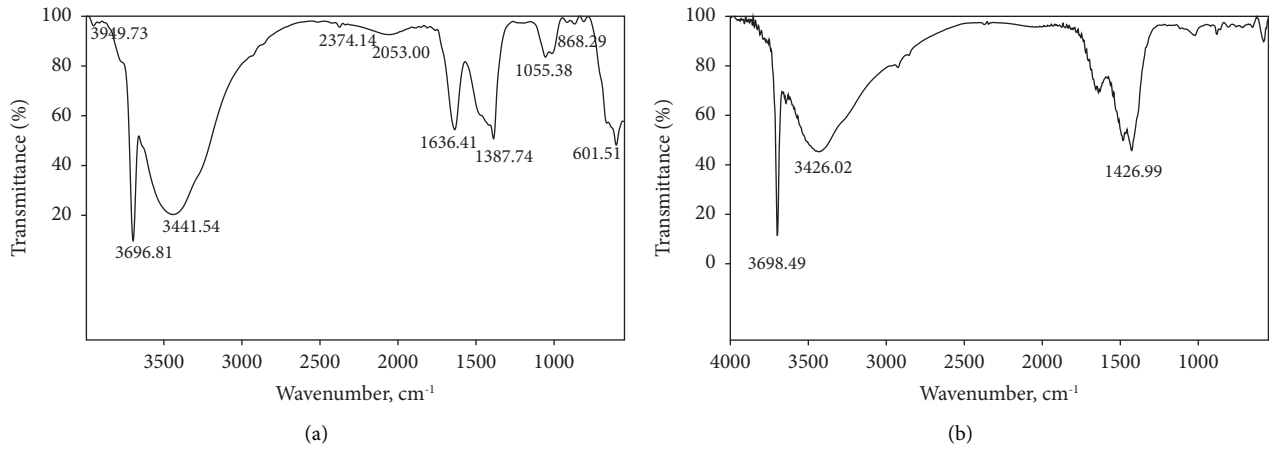


FIGURE 2: (a) FTIR of n-GO; (b) FTIR of UV/n-GO.

TABLE 1: Levels of different process variables in coded and uncoded forms for adsorption.

Variables	Name of the process variables	Ranges and levels				
		-2	-1	0	1	2
A	Time, min	10	20	30	40	50
B	Adsorbent dosage, w , g/L	0.1	0.2	0.3	0.4	0.5
C	Initial concentration of dye in the aqueous solution, C_0 , mg/L	10	15	20	25	30
D	pH of the aqueous solution	5	6	7	8	9

TABLE 2: Actual versus model predicted values for adsorption.

Run	A, time (min)	B, w (g/L)	C, C_0 mg/L	D, pH	% adsorption experimental	% adsorption predicted
1	40	0.2	15	8	88.65	88.93
2	20	0.4	25	8	88.91	89.53
3	30	0.3	20	7	91.91	91.65
4	20	0.2	15	6	94.26	94.70
5	30	0.5	20	7	90.42	90.37
6	30	0.3	20	7	92.4	91.65
7	30	0.1	20	7	93.44	92.94
8	40	0.4	15	6	89.28	89.13
9	40	0.4	25	8	91.4	91.13
10	20	0.2	25	8	90.12	90.44
11	20	0.4	15	6	93.26	93.71
12	30	0.3	20	7	92.4	91.65
13	30	0.3	30	7	92.4	92.49
14	30	0.3	20	9	90	89.69
15	50	0.3	20	7	90	90.50
16	40	0.2	25	6	94.66	95.12
17	20	0.4	25	6	91.71	91.60
18	40	0.4	15	8	84.64	84.99
19	30	0.3	20	7	91.66	91.65
20	30	0.3	20	7	91.66	91.65
21	30	0.3	10	7	90.75	90.82
22	40	0.2	15	6	91	90.78
23	40	0.2	25	8	92.78	92.73
24	10	0.3	20	7	92.95	92.81
25	30	0.3	20	7	91.66	91.65
26	20	0.2	25	6	90.17	90.22
27	40	0.4	25	6	95.72	95.82
28	20	0.4	15	8	92.47	92.18
29	30	0.3	20	5	93.8	93.62
30	20	0.2	15	8	95.15	95.45

perform analysis of variance (ANOVA). The probability values (P values) were used to perform as a device to check the significance of each coefficient, which also showed the interaction strength of each parameter. The smaller the P values, the bigger the significance of the corresponding coefficient. Table 3 presents the ANOVA results for the study.

The model's F -value of 77.06 indicates that it is significant. An F -value this big may arise owing to noise just 0.01% of the time. Model terms are significant if the P value is less than 0.0500. AC, AD, BC, and BD are the key model terms in this scenario. Values larger than 0.1000 imply that the model terms are unimportant. Model reduction may enhance your model if it has a large number of irrelevant model terms (except those necessary to maintain hierarchy). The lack of fit F -value of 1.53 indicates that the lack of fit is insignificant in comparison to the pure error. A significant lack of fit F -value owing to noise has a 33.67% chance of occurring [28].

Table 4 presents the key quality parameters to check the adequacy of the model. The coefficient of determination (R^2) was found to be 0.9759, suggesting that the model explained 97.59% of the experimental data and only 2.41% of the overall variations. A high R^2 number, in general, indicates a strong match between expected and experimental outcomes. With a value of 0.9633, the adjusted coefficient of determination ($\text{Adj}R^2$) was found to be very high, meaning that the model accounted for 96.33% of the observed variability. The coefficient of variation (C.V. %) was found to be 0.4668, indicating that the difference between the expected and experimental results was limited, implying that the experiment was precise and dependable. The adjusted R^2 of 0.9633 is reasonably close to the predicted R^2 of 0.9215; that is, the difference is less than 0.2. The signal-to-noise ratio is measured by adeq precision. It is preferable to have a ratio of more than four. A signal-to-noise ratio of 41.802 indicates a good signal. The design space may be navigated using this concept.

3.2.2. Final Equation in Terms of Coded Factors. The equation in terms of coded factors can be used to make predictions about the response for given levels of each factor. By default, the high levels of the factors are coded as +1 and the low levels are coded as -1. The coded equation is useful for identifying the relative impact of the factors by comparing the following factor coefficients:

$$\begin{aligned} \% \text{Removal} = & +91.65 - 0.5758A - 0.6433B + 0.4192C \\ & - 0.9808D - 0.1687AB + 2.20AC \\ & + 0.6525AD + 0.5887BC \\ & - 0.5725BD - 0.1350CD. \end{aligned} \quad (2)$$

3.2.3. Diagnostic Case Plots: Residual versus Predicted Plot. For the model to be valid and the assumptions to be met, the residual value must be structured less. In particular, it must be unconnected with any other variable, including the anticipated response. Plotting the residual vs. the fitted

(predicted) values is a straightforward check. The assumption of constant variance is tested with a plot of the residual vs. the rising anticipated response values. As demonstrated in Figure 3, the plot indicates random scatter or structureless, which fulfills the premise of constant variance.

3.2.4. Response Surface Plots and Interactions between the Adsorption Parameters for Adsorption. The response surface 3D surface contour plots of % adsorption vs. interaction effects of agitation duration, dye concentration, adsorbent dosage, and aqueous solution pH are shown in Figures 4(a)–4(d). Each contour plot depicts a variety of various test parameter combinations, with the other value set to zero. The maximum % adsorption was found on the surface enclosed in the contour plot's smallest curve (circular or elliptical). The nonlinear nature of the resulting interactive plot of the agitation time and the starting concentration, as shown in Figure 4(a), implies that the % removal is influenced by the interaction graph of the initial concentration and the agitation duration. As seen in the graph, extending the agitation time from 20 to 30 min enhances the % removal rate, and the % removal rate improves as the starting concentration rises. Due to possible dye-molecule interaction, the % clearance declined as the initial dye concentration was increased further.

Figure 4(b) depicts the interaction effect of time and pH; at greater pH and time, the % removal decreases. The % removal rate is negatively affected by basic conditions, and MB removal is greatest near the neutral pH level. Figure 4(c) shows that once the dosage exceeds 0.25 g/L, the MB clearance declines at lower MB concentrations due to total saturation. The 3D response plot (Figure 4(d)) demonstrates that increasing the pH of the solution as well as the dose decreased MB adsorption. With a dosage in the range of 0.3–0.4 g/L at pH > 7.0, the adsorption efficiency decreased and then remained nearly constant. The transfer of an excess proton to the reactive centre resulted in the appearance of more repulsive electrostatic forces, resulting in a fall in removal %.

3.2.5. Optimization. In the process optimization, % removal may be improved or maximized by adjusting process parameters such as agitation duration, adsorbent dose, dye concentration, and pH. The feature of desirability was used in Design Expert software version 11.0 to maximize the answer. In this study, numerical optimization was chosen because it provides a thorough and up-to-date explanation of the most successful process optimization approaches. To do so, the upper and lower limits of each variable, as well as its anticipated response by the model, were supplied using the previously generated contour and surface plots. The final objective of this optimization was to achieve the best possible response by reducing the model variables. Figure 5 depicts the desirability profile for % removal vs. factors. The desirability scale ranges from 0.0 to 1.0, corresponding to the transition from an unpleasant to a much desired state. The best circumstances were established by considering % removal to be maximized, which were a pH of 6, a dose of

TABLE 3: ANOVA table for the model to predict % removal.

Sources	Sum of squares	Df	Mean square	F-value	P value
Model	141.07	10	14.11	77.06	<0.0001 significant
A time	7.96	1	7.96	43.47	<0.0001
B dosage	9.93	1	9.93	54.26	<0.0001
C initial concentration	4.22	1	4.22	23.04	0.0001
D pH	23.09	1	23.09	126.13	<0.0001
AB	0.4556	1	0.4556	2.49	0.1312
AC	77.53	1	77.53	423.51	<0.0001
AD	6.81	1	6.81	37.21	<0.0001
BC	5.55	1	5.55	30.30	<0.0001
BD	5.24	1	5.24	28.65	<0.0001
CD	0.2916	1	0.2916	1.59	0.2222
Residual	3.48	19	0.1831		
Lack of fit	2.82	14	0.2014	1.53	0.3367 not significant
Pure error	0.6589	5	0.1318		
Cor total	144.55	29			

TABLE 4: Model adequacy measure.

Std. dev.	0.4279	R^2	0.9759
Mean	91.65	Adjusted R^2	0.9633
C.V. %	0.4668	Predicted R^2	0.9215
		Adeq precision	41.8019

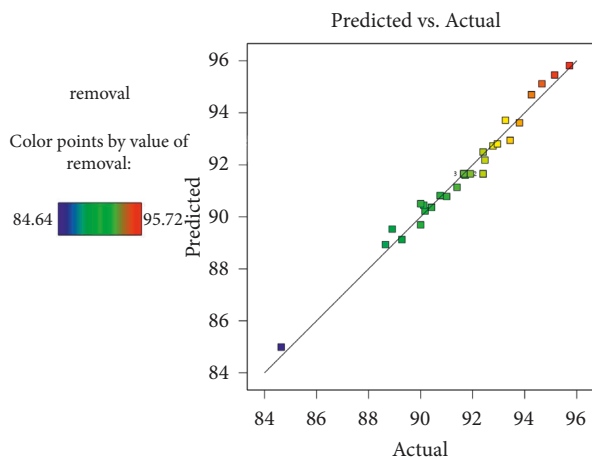


FIGURE 3: Comparison plot between the experimental data and predicted data for adsorption.

0.4 g/L, a starting dye concentration of 25 mg/L, and a period of 40 min. The removal rate was 95.81%, with an overall desirability of 0.853. A comparison study was performed for the plain n-GO sample under the optimal conditions; i.e., a pH of 6, a dose of 0.4 g/L, a starting dye concentration of 25 mg/L, and a period of 40 min gave 90.6% MB removal.

3.2.6. Validation of the Model. An experiment involving process variables was carried out to examine the impacts of experimental design parameters based on the central composite design outcome. As shown in Figure 5, numerical optimization was used to enhance the % removal of dye. According to the results of the research, the ideal %

reduction was 95.96%. This is in line with what was expected. As a consequence, the model was deemed accurate and trustworthy for forecasting % removal from the adsorbent.

3.3. ANN Modeling Using MATLAB. The testing dataset's maximum R^2 and smallest MSE values were utilized to establish the optimum design of an ANN model. The standard backpropagation technique was used to optimize the training process. The optimum adsorption structure was discovered to be 4-4-1, and the design is shown in Figure 6.

The modelling results yielded R^2 and MSE values of 0.9572 and 0.00012, respectively. The ANN model obtained a strong connection to the optimal structure from the training data, as shown in Figure 7(a), and it performed quite well in validation and testing despite some data scattering (Figures 7(b) and 7(c)). As seen in Fig, for the adsorption dataset (Figure 7(d)), the ANN model performed brilliantly. In Figure 8, the MSE for the improved ANN model is shown vs. the epoch number. The training process was discovered to have ended after 18 epochs. All of these observations demonstrated that the experimental data and the predicted data from the ANN model agreed well. The ANN model predicted 94.76% removal as the maximum % removal under the optimal conditions specified by RSM.

3.4. Adsorption Kinetics. The kinetics of adsorption were investigated to explain the dynamics of the adsorption process after fitting the data to pseudo-first-order, pseudo-second-order, and Elovich models (Figure 9(a)). Table 5 displays the experimental data for the models, as well as the model parameters and constants for each model. The kinetic investigations were carried out in MB aqueous solutions of 25 mg/L concentration at pH = 6 and temperature = 303 K and an adsorbent dosage of 0.4 g/L. The adsorption efficiency rose up to 30 min before becoming constant. This might be due to the large number of open accessible sites that gradually get saturated when a monolayer of metal ions forms on the adsorbent surface. As a result, the optimal time

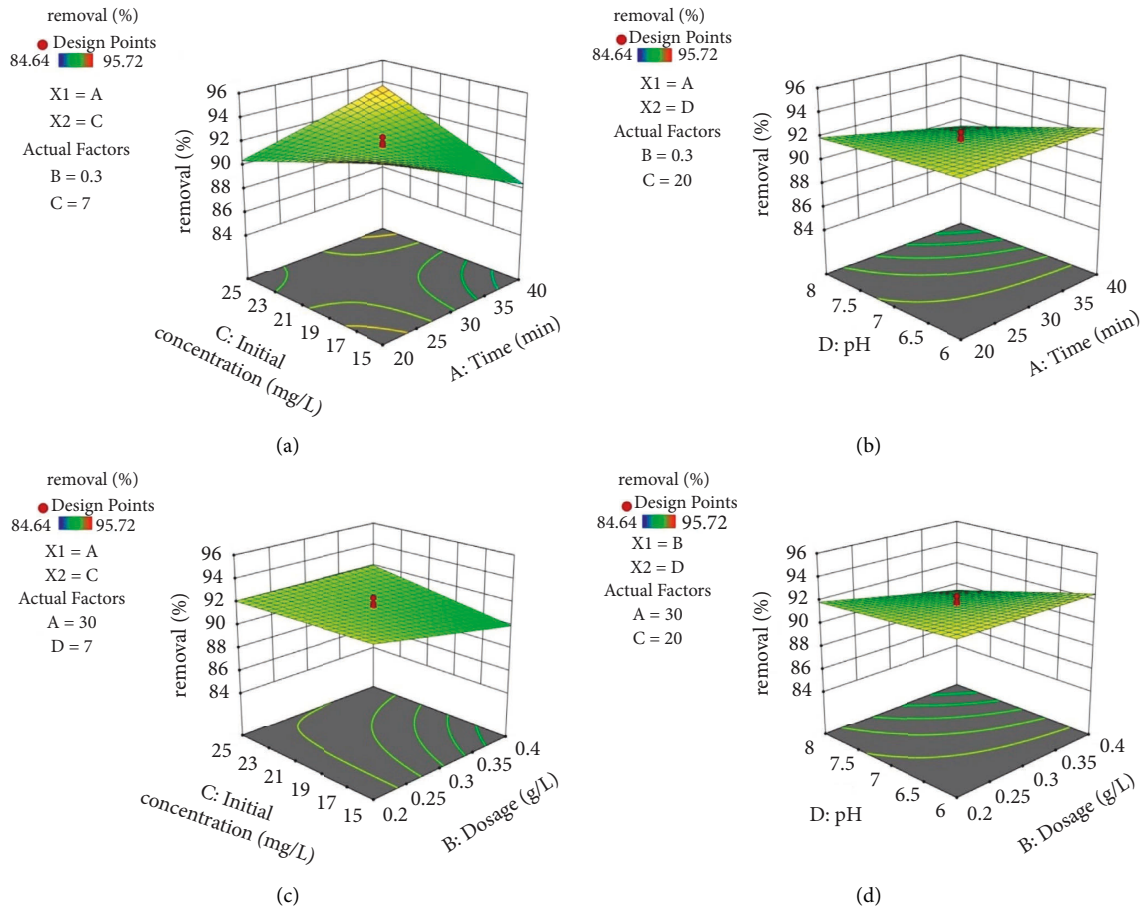


FIGURE 4: 3D response surface plots for adsorption: (a) time vs. initial concentration, (b) time vs. pH, (c) concentration vs. dosage, and (d) pH vs. dosage.

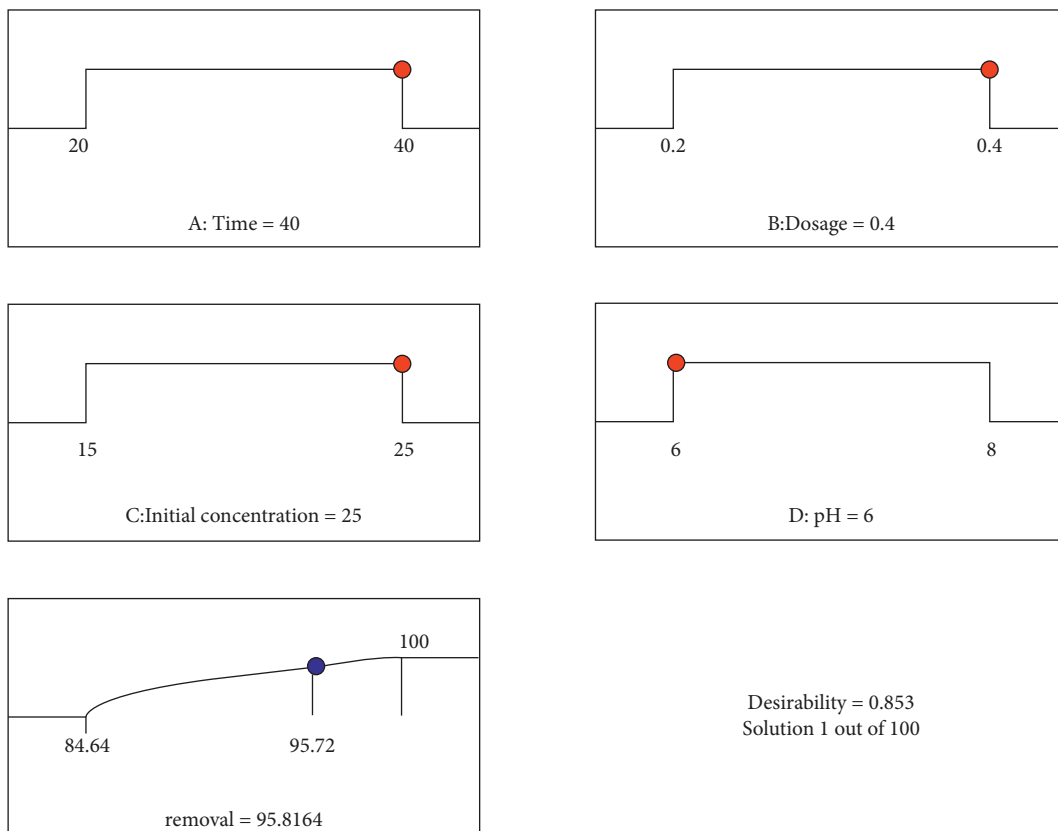


FIGURE 5: Desirability plot for adsorption.

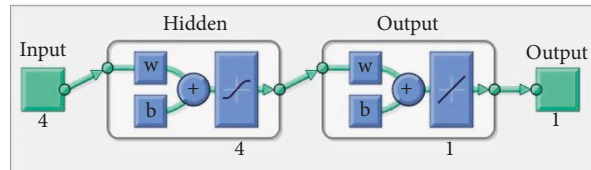


FIGURE 6: Optimum ANN architecture.

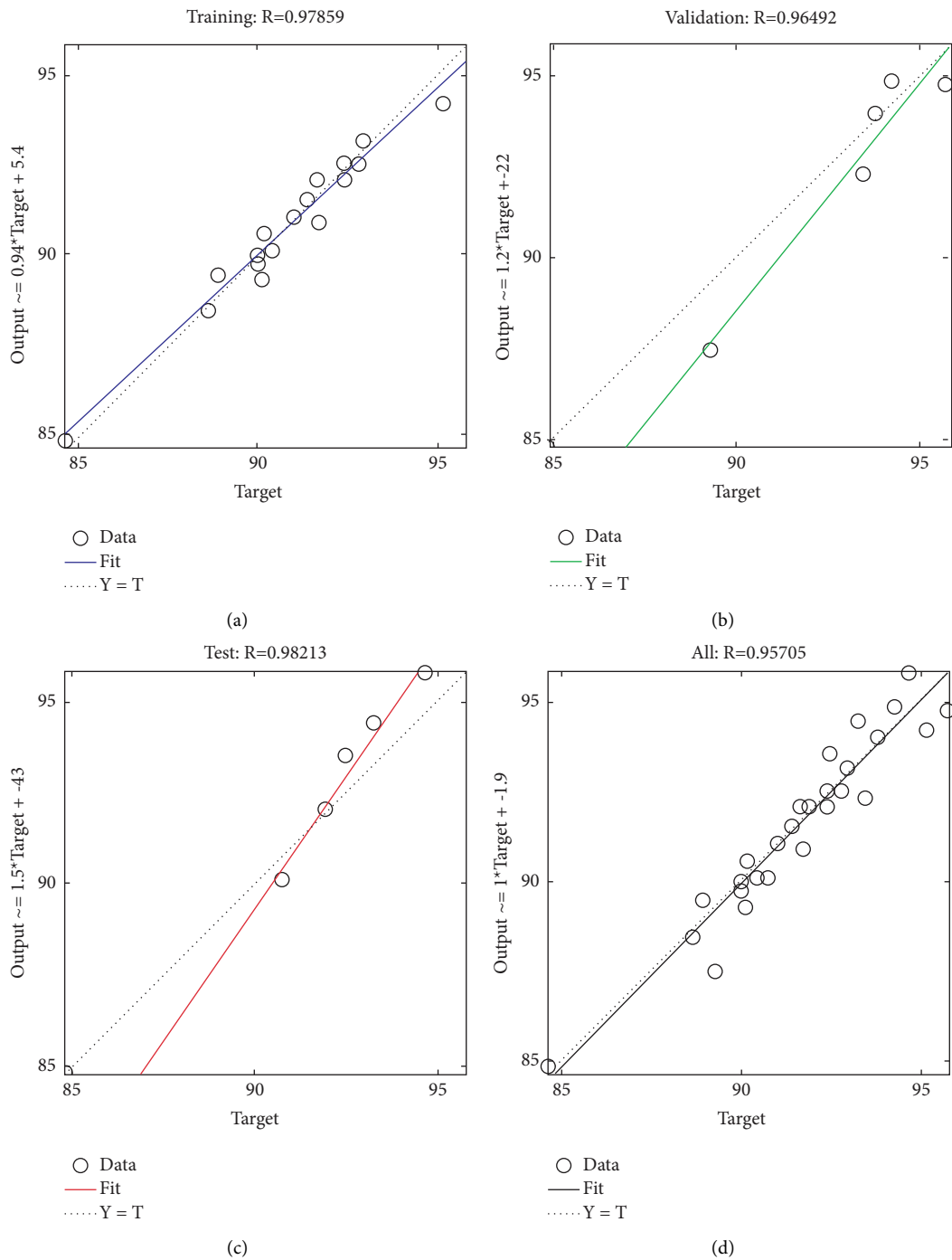


FIGURE 7: Output of the ANN model: (a) training, (b) validation, (c) testing, and (d) complete data.

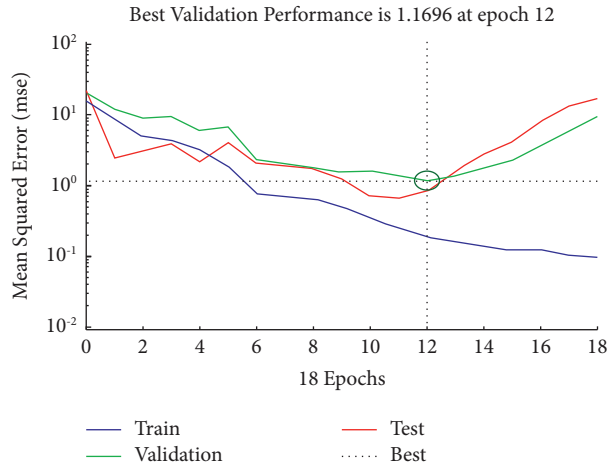


FIGURE 8: MSE vs. the number of epochs in the hidden layer.

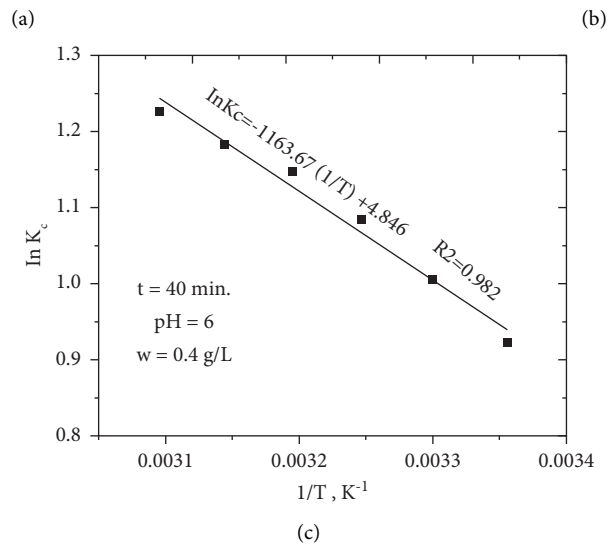
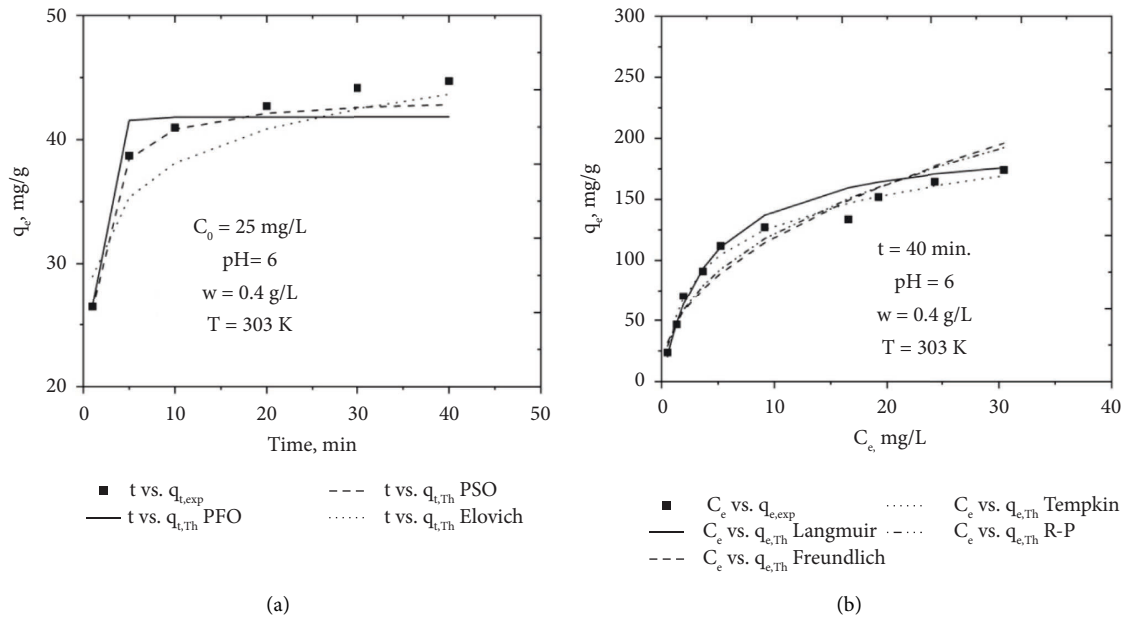


FIGURE 9: (a) Kinetic studies. (b) Equilibrium studies. (c) Thermodynamic studies for adsorption of MB by UV/n-GO.

TABLE 5: Kinetic parameters and their correlation coefficients calculated for the adsorption of MB by UV/n-GO (pH = 6; dosage = 0.4 g/L; concentration = 25 mg/L; temperature = 303 K).

Models	Equations	Parameters	Values
Pseudo-first order	$q_t = q_e (1 - e^{-k_1 t})$	$k_1 (\text{min}^{-1})$	1.007
		$q_e (\text{calc}) \text{mg/g}$	41.81
		R^2	0.899
		χ^2	0.5599
Pseudo-second order	$q_t = q_e^2 k_2 t / (1 + q_e k_2 t)$	$k_2 (\text{g}/(\text{mg}\cdot\text{min}))$	0.0349
		$q_e (\text{calc}) \text{mg/g}$	43.5
		R^2	0.9719
		χ^2	0.1545
Elovich	$q_t = \ln(1 + \alpha\beta t) / \beta$	$\beta (\text{g}/\text{mg})$	0.2514
		$\alpha (\text{mg}/\text{g}\cdot\text{min})$	5757.84
		R^2	0.8572
		χ^2	0.9263
		$q_e (\text{Exp.}) \text{mg/g}$	44.35

period was determined to be 30 min. Because of the large difference between the predicted and actual values of q_e , and $R^2 = 0.899$, the pseudo-first-order kinetic model is ineffective for fitting the experimental data. The use of pseudo-second-order kinetics was demonstrated to be useful in interpreting experimental findings concerning MB adsorption by the adsorbent with high R^2 values (0.9719) and low χ^2 (chi-square) values (0.1545). The Elovich model was used to analyze the nature of diffusion kinetics, and it is found to be fitting well with the experimental data ($R^2 = 0.8572$), as evidence that the rate determining step is not totally diffusion in nature, but it has a modest effect on the adsorption process. The MB adsorption fits the Elovich model well, with an initial rate constant (α) of 5757.84 mg/g.min and a low desorption rate constant ($\beta = 0.2514$ g/mg).

3.5. Equilibrium Studies. To fully comprehend adsorbate-adsorbent interactions, the adsorption capacity of UV/n-GO under various circumstances must be meticulously determined. The experimental data collected in this work were fitted into four equilibrium models, i.e., Langmuir, Freundlich, Temkin, and Redlich–Peterson isotherms (Figure 9(b)). Table 6 includes the isotherm constants and correlation coefficients (R^2 , χ^2). With high R^2 and low χ^2 values, the Langmuir isotherm demonstrates that it is the best model to reflect equilibrium. The highest monolayer adsorption capacity (q_{max}) for MB removal determined by Langmuir was 200 mg/g. Based on the separation factor R_L values ($R_L = 1/(1 + K_L C_0)$), the adsorption process may be rated as favorable, where K_L (L/mg) is the Langmuir constant and C_0 is the initial adsorbate concentration (mg/L). The Freundlich isotherm, unlike the Langmuir equation, cannot capture either the linearity range at very low concentrations or the saturation impact at very high concentrations. The Freundlich constant (n), often known as the adsorption intensity factor or surface heterogeneity, shows whether or not the adsorption is favorable. A value for the Freundlich constant “ n ” in between 0 and 1 (0.446) indicates the adsorption is favorable. The Temkin isotherm takes into account adsorbent-adsorbate interactions. The model assumes that the heat of adsorption (a function of

temperature) of all molecules in the layer decreases linearly rather than logarithmically with coverage by neglecting extremely low and high concentration values. When the equilibrium data are fitted to the Temkin model, the heat of adsorption (b) is calculated to be 68.82 J/mol. The Temkin constant ($B = RT/b$) and the equilibrium binding constant (K_T) of 3.3346 L/mg are used to compute this. The results suggest that adsorbent-adsorbate interactions can lower the adsorption heat. As a result, dye adsorption displayed a continuous spectrum of binding energies that ranged from zero to the greatest practical value. Given the limitations of the Freundlich and Langmuir isotherms, the Redlich–Peterson isotherm with three parameters was proposed. This model combines aspects of the Freundlich and Langmuir models and may be useful for displaying adsorption equilibrium over a wide range of adsorbate concentrations. The R–P isotherm constant “ g ” value of 0.61 indicates that the model was approaching the Langmuir isotherm.

3.5.1. Thermodynamics. Thermodynamic studies are the sole method that can be used to forecast adsorption processes (e.g., physical and chemical). Thermodynamics parameters (energy and entropy) are used to determine the spontaneity of an adsorption process. In environmental applications, energy and entropy are two topics that need to be discussed to properly evaluate the spontaneous nature of certain processes. The changes in free energy (ΔG^0), enthalpy (ΔH^0), and entropy (ΔS^0) of the adsorption process were determined. The well-known Van’t Hoff equation is as follows:

$$\ln K_C = -\frac{\Delta H^0}{R} \left(\frac{1}{T} \right) + \frac{\Delta S^0}{R}. \quad (3)$$

The result of Van’t Hoff’s plot of $\ln(K_C)$ as a function of $1/T$ is a straight line, which can be seen in Figure 9(c). The slope and intercept of this line were used to determine ΔH^0 and ΔS^0 , respectively. The Van’t Hoff thermodynamic analysis showed that the adsorption of MB was spontaneous (with a negative Gibbs free energy, denoted by ΔG^0) and endothermic (with a positive enthalpy change, denoted by

TABLE 6: Isotherm constants and their correlation coefficients for the adsorption of MB by UV/n-GO (agitation time = 40 min, pH = 6, dosage = 0.4 g/L, and temperature = 303 K).

Models	Equations	Parameters	Values
Langmuir	$q_e = q_{\max} k_L C_e / (1 + k_L C_e)$	$q_{\max}(\text{mg/g})$	200
		$k_L(\text{L/mg})$	0.238
		R_L	0.2957–0.0138
		R^2	0.9791
		χ^2	7.1244
Freundlich	$q_e = K_F C_e^n$	n	0.446
		$K_F (\text{mg/g})/(\text{mg/L})^n$	42.657
		R^2	0.9579
		χ^2	20.432
Temkin	$q_e = B \ln(C_e K_T)$	B	36.6
		$K_T(\text{L/mg})$	3.3346
		R^2	0.9929
		χ^2	3.808
R–P	$q_e = k_{rp} C_e / (1 + a_{rp} C_e^g)$	$k_{rp} (\text{L/g})$	157.332
		$a_{rp} ((\text{mg/L})^{-g})$	2.7731
		g	0.631
		R^2	0.998
		χ^2	14.5867

ΔH°), with the solid-liquid interface undergoing randomness during the reaction (denoted by entropy, denoted by ΔS°).

4. Conclusions

The objective of the present research is to synthesize UV-treated nano-graphene oxide and adsorption for the removal of a cationic dye, i.e., methylene blue. The adsorption studies were carried out with the design of experiments (DOE) methodology. ANN modelling was carried out with MATLAB.

- (i) A chemical method was used for the synthesis of graphene oxide nanoparticles.
- (ii) A cost-effective physical treatment, i.e., UV irradiation was employed for the modification of n-GO.
- (iii) The crystallite size of the samples was estimated from the XRD analysis by using the Debye–Scherrer formula; i.e., n-GO is 13.2 nm and UV/n-GO is 12.42 nm.
- (iv) FTIR spectra were recorded which show the presence of the IR peaks.
- (v) SEM images confirmed that the sizes of all synthesized samples are in the range of nanoscale and are in accordance with XRD results with spherical morphology of the particles.
- (vi) % MB removal of the optimal variables by CCD-RSM was found to be 95.81% with an overall desirability of 0.728.
- (vii) The ANN model was developed with MATLAB revealing that the experimental data and the anticipated data from the ANN model were in good agreement, and % MB removal at the optimal variables by ANN was found to be 94.76%

(viii) The pseudo-second order model had a better fit for the adsorption kinetics than any other model. The equilibrium may be well explained using the Langmuir isotherm. The maximum adsorption capacity of 200 mg/g was achieved. According to thermodynamic research, the adsorption process produces an endothermic reaction.

(ix) Based on the findings of the experiments, it is possible to draw the conclusion that UV functionalization of nano-graphene oxide renders it an efficient adsorbent, and as a result, it is suitable for further research in the form of scale-up studies.

Data Availability

All the data are available in the manuscript.

Conflicts of Interest

The authors declare that they have no conflicts of interest.

References

- [1] R. Senthilkumar, D. M. Reddy Prasad, L. Govindarajan, K. Saravanakumar, and B. S. Naveen Prasad, "Synthesis of green marine algal-based biochar for remediation of arsenic(V) from contaminated waters in batch and column mode of operation," *International Journal of Phytoremediation*, vol. 22, no. 3, pp. 279–286, 2020.
- [2] V. R. Myneni, T. Punugoti, N. S. Kala, N. R. Kanidarapu, and M. Vangalapati, "Modelling and optimization of methylene blue adsorption onto magnesium oxide nanoparticles loaded onto activated carbon (MgONP-AC): response surface methodology and artificial neural networks," *Materials Today Proceedings*, vol. 18, pp. 4932–4941, 2019.
- [3] K. Saravanakumar, R. Senthilkumar, D. M. R. Prasad, B. S. N. Prasad, S. Manickam, and V. Gajendiran, "Batch and column arsenate sorption using turbinaria ornata seaweed derived biochar: experimental studies and mathematical

- modeling,” *ChemistrySelect*, vol. 5, no. 12, pp. 3661–3668, 2020.
- [4] J. H. Deng, X. R. Zhang, G. M. Zeng, J. L. Gong, Q. Y. Niu, and J. Liang, “Simultaneous removal of Cd(II) and ionic dyes from aqueous solution using magnetic graphene oxide nanocomposite as an adsorbent,” *Chemical Engineering Journal*, vol. 226, pp. 189–200, 2013.
- [5] M. V. Ratnam, C. Karthikeyan, K. N. Rao, and V. Meena, “Magnesium oxide nanoparticles for effective photocatalytic degradation of methyl red dye in aqueous solutions: optimization studies using response surface methodology,” *Materials Today Proceedings*, vol. 26, pp. 2308–2313, 2020.
- [6] V. R. Myneni, N. R. Kanidarapu, and M. Vangalapati, “Methylene blue adsorption by magnesium oxide nanoparticles immobilized with chitosan (CS-MgONP): response surface methodology, isotherm, kinetics and thermodynamic studies,” *Iranian journal of chemistry and chemical engineering*, vol. 39, no. 6, pp. 29–42, 2020.
- [7] N. M. Mahmoodi and H. D. Mohammad, “Clean Laccase immobilized nanobiocatalysts (graphene oxide - zeolite nanocomposites): from production to detailed biocatalytic degradation of organic pollutant,” *Applied Catalysis B*, vol. 268, Article ID 118443, 2020.
- [8] H. Guo, T. Jiao, Q. Zhang, W. Guo, Q. Peng, and X. Yan, “Preparation of graphene oxide-based hydrogels as efficient dye adsorbents for wastewater treatment,” *Nanoscale Research Letters*, vol. 10, no. 1, pp. 272–279, 2015.
- [9] S. Shang, Z. Tao, C. Yang et al., “Facile synthesis of CuBTC and its graphene oxide composites as efficient adsorbents for CO₂ capture,” *Chemical Engineering Journal*, vol. 393, Article ID 124666, 2020.
- [10] N. M. Mahmoodi, A. Taghizadeh, M. Taghizadeh, and M. Azimi Shahali Baglou, “Surface modified montmorillonite with cationic surfactants: preparation, characterization, and dye adsorption from aqueous solution,” *Journal of Environmental Chemical Engineering*, vol. 7, no. 4, Article ID 103243, 2019.
- [11] Y. Wang, W. Xie, H. Liu, and H. Gu, “Hyperelastic magnetic reduced graphene oxide three-dimensional framework with superb oil and organic solvent adsorption capability,” *Advanced Composites and Hybrid Materials*, vol. 3, no. 4, pp. 473–484, 2020.
- [12] M. Ghorbanpour, A. H. Khaltabadi Farahani, and J. Hadian, “Potential toxicity of nano-graphene oxide on callus cell of *Plantago major* L. under polyethylene glycol-induced dehydration,” *Ecotoxicology and Environmental Safety*, vol. 148, pp. 910–922, 2018.
- [13] S. Rodríguez-García, R. Santiago, D. Lopez-Diaz et al., “Role of the structure of graphene oxide sheets on the CO₂ adsorption properties of nanocomposites based on graphene oxide and polyaniline or Fe₃O₄-nanoparticles,” *ACS Sustainable Chemistry & Engineering*, vol. 7, no. 14, 2019.
- [14] C. M. Park, D. Wang, J. Han, J. Heo, and C. Su, “Evaluation of the colloidal stability and adsorption performance of reduced graphene oxide-elemental silver/magnetite nanohybrids for selected toxic heavy metals in aqueous solutions,” *Applied Surface Science*, vol. 471, 2019.
- [15] S. Kandasamy, N. K. Manickam, K. Subbiah, K. Muthukumar, M. Kumaraguruparaswami, and M. Venkata Ratnam, “Nanotechnology’s contribution to next-generation bio-energy production,” in *Nanomaterials*, R. P. Kumar and B. B. T.-N. Bharathiraja, Eds., pp. 511–518, Academic Press, Cambridge, MA, USA, 2021.
- [16] M. Heidarizad and S. S. Şengör, “Synthesis of graphene oxide/magnesium oxide nanocomposites with high-rate adsorption of methylene blue,” *Journal of Molecular Liquids*, vol. 224, pp. 607–617, 2016.
- [17] C. S. Cheng, J. Deng, B. Lei et al., “Toward 3D graphene oxide gels based adsorbents for high-efficient water treatment via the promotion of biopolymers,” *Journal of Hazardous Materials*, vol. 263, pp. 467–478, 2013.
- [18] M. Oveisi, M. Alinia Asli, and N. M. Mahmoodi, “Carbon nanotube based metal-organic framework nanocomposites: synthesis and their photocatalytic activity for decolorization of colored wastewater,” *Inorganica Chimica Acta*, vol. 487, pp. 169–176, 2019.
- [19] G. Z. Kyzas, E. A. Deliyanni, and K. A. Matis, “Graphene oxide and its application as an adsorbent for wastewater treatment,” *Journal of Chemical Technology and Biotechnology*, vol. 89, no. 2, pp. 196–205, 2014.
- [20] A. M. Varghese, K. S. K. Reddy, S. Singh, and G. N. Karanikolos, “Performance enhancement of CO₂ capture adsorbents by UV treatment: the case of self-supported graphene oxide foam,” *Chemical Engineering Journal*, vol. 386, Article ID 124022, 2020.
- [21] C. E. Onu, J. T. Nwabanne, P. E. Ohale, and C. O. Asadu, “Comparative analysis of RSM, ANN and ANFIS and the mechanistic modeling in eriochrome black-T dye adsorption using modified clay,” *South African Journal of Chemical Engineering*, vol. 36, pp. 24–42, 2021.
- [22] C. K. Rojas-Mayorga, I. A. Aguayo-Villarreal, J. Moreno-Pérez, R. Muñoz-Valencia, M. Á. Montes-Morán, and R. Ocampo-Pérez, “Influence of calcium species on SO₂ adsorption capacity of a novel carbonaceous materials and their ANN modeling,” *Journal of Environmental Chemical Engineering*, vol. 9, no. 1, Article ID 104810, 2021.
- [23] L. Wu, X. Liu, G. Lv et al., “Study on the adsorption properties of methyl orange by natural one - dimensional nano - mineral materials with different structures,” *Scientific Reports*, vol. 11, Article ID 106401, 2021.
- [24] N. M. Mahmoodi, F. Najafi, and A. Neshat, “Poly (amido-amine-co-acrylic acid) copolymer: synthesis, characterization and dye removal ability,” *Industrial Crops and Products*, vol. 42, pp. 119–125, 2013.
- [25] K. Gupta and O. P. Khatri, “Reduced graphene oxide as an effective adsorbent for removal of malachite green dye: plausible adsorption pathways,” *Journal of Colloid and Interface Science*, vol. 501, pp. 11–21, 2017.
- [26] A. T. Habte, D. W. Ayele, and M. Hu, “Synthesis and characterization of reduced graphene oxide (rGO) started from graphene oxide (GO) using the tour method with different parameters,” *Advances in Materials Science and Engineering*, vol. 2019, Article ID 5058163, 9 pages, 2019.
- [27] N. M. Mahmoodi, M. Oveisi, M. Bakhtiari et al., “Environmentally friendly ultrasound-assisted synthesis of magnetic zeolitic imidazolate framework - graphene oxide nanocomposites and pollutant removal from water,” *Journal of Molecular Liquids*, vol. 282, pp. 115–130, 2019.
- [28] G. Tadesse, *Valorization of Coffee Husk To Bio-Ethanol Using Shf Method*, Addis Ababa University, Addis Ababa, Ethiopia, 2018.